Striated drifting auroral kilometric radiation bursts: Possible stimulation by upward traveling EMIC waves

J. D. Menietti,[1] R. L. Mutel,[1] O. Santolik,[2,3] J. D. Scudder,[1] I. W. Christopher,[1] and J. M. Cook[1]

Received 26 July 2005; revised 23 December 2005; accepted 20 January 2006; published 21 April 2006.

[1] We investigate waves observed by the Cluster wideband instrument (WBD) during an orbital conjunction with the Polar spacecraft. During this perigee pass, Polar was at the upper extent of the auroral kilometric radiation (AKR) source region in the Southern Hemisphere nightside auroral region. Cluster was located at higher altitude above this region and observed AKR with clear signatures of ordered fine structure striations (rain). Using electron particle data observed by HYDRA on board Polar, we have modeled the electron distribution function within the AKR source region. This distribution function is unstable to a number of low-frequency wave modes and supports EMIC waves propagating along the magnetic field line. These waves appear to be feasible to stimulate the growth of AKR, producing the ordered fine structure observed by WBD on board Cluster, but further analysis will be important, especially plasma simulations.

Citation: Menietti, J. D., R. L. Mutel, O. Santolik, J. D. Scudder, I. W. Christopher, and J. M. Cook (2006), Striated drifting auroral kilometric radiation bursts: Possible stimulation by upward traveling EMIC waves, *J. Geophys. Res.*, *111*, A04214, doi:10.1029/2005JA011339.

1. Introduction and Background

[2] *Gurnett et al.* [1979] and *Gurnett and Anderson* [1981] using ISEE data, *Benson et al.* [1988] using DE-1 data, and *Morioka et al.* [1981] with EXOS-B data have all reported examples of auroral kilometric radiation (AKR) fine structure in both the ordinary and extraordinary modes, indicating that AKR is emitted in discrete bursts lasting only a few seconds or less. Observed frequency drift rates of features are in the range 100 Hz s^{-1} to 10's of kHz s^{-1}. The fractional bandwidth can be quite small ($\sim 10^{-3}$ or less). *Gurnett et al.* [1979] suggest that the drifting features may be due to rising and falling source regions. The fine structures include not only drifting features but also discrete bands of near-monochromatic emission and other discrete features that are seen at the highest resolution available.

[3] There are a number of theories which attempt to explain the source of AKR fine structure. Such knowledge is necessary if we are to fully understand the details of the AKR generation mechanism. *Wu and Lee* [1979] have no doubt correctly identified the electron cyclotron maser as the plasma instability mechanism responsible for the emission, but as pointed out some years ago by *Melrose* [1986], this mechanism would be an incomplete theory if it could not explain the timescales of wave growth associated with AKR fine structure.

[4] *Pottelette et al.* [2001] have proposed that electron holes in the AKR source region are the source of the AKR fine structure. These authors envision the electron holes as elementary radiation centers. They estimate the power levels at 10^3 to 10^4 W per electron hole. Given that estimates of the total AKR power are typically 10^8 to 10^9 W or higher, this theory requires a large number of electron holes to explain the aggregate AKR fine structure. The authors argue that electron holes are reflected by the acceleration potential or are trapped within ion acoustic waves or ion holes to produce the array of seemingly random signatures on frequency versus time spectrograms. Electron holes have been observed abundantly in the downward current regions but only sparsely in the upward current regions, the source region of AKR [cf. *Ergun et al.*, 1998a, 1999]. This has led *Pottelette et al.* [1999] to suggest that the AKR fine structure is generated at the edge of the ionospheric cavity region, where nonlinear electron acoustic waves may be excited. More recently, *Pottelette and Treumann* [2005] report that electron holes are observed by FAST in the upward current region in the form of "tripolar" structures. The observed structures are believed to move away from the Earth at velocities in the range 40 to 100 km s^{-1}. *Pottelette and Treumann* [2005] suggest these structures are responsible for the random AKR fine structure but not the ordered AKR fine structure striations. *Mutel et al.* [2006] argue that ion holes, rather than electron holes or tripolar structures, are the source of AKR ordered fine structure.

[5] Auroral ROAR is a relatively narrowband emission occurring near twice the electron gyrofrequency and first detected by *Kellogg and Monson* [1979]. *LaBelle et al.* [1995] and *Shepherd et al.* [1996] have reported similar

[1]Department of Physics and Astronomy, University of Iowa, Iowa City, Iowa, USA.
[2]Faculty Mathematics and Physics, Charles University, Prague, Czech Republic.
[3]Also at Institute of Atmospheric Physics, Czech Academy of Sciences, Prague, Czech Republic.

0148-0227/06/2005JA011339$09.00

structures in auroral ROAR emissions at frequencies of a few MHz (2 or 3 times the local gyrofrequency). The signatures include a series of "multiple discrete features" with positive and negative slope on a frequency-time spectrogram. These signatures are similar to those described by *Menietti et al.* [1996] in the AKR fine structure as ordered fine structure (OFS) or "rain" and postulated as stimulated emission. The relationship, if any, between the auroral ROAR discrete signatures and the AKR striations is not known. We point out that auroral roar is believed to be due to a mode-conversion mechanism analogous to terrestrial continuum emission rather than to AKR.

[6] *Menietti et al.* [1996] suggested that negative-slope striated bursts are produced by stimulation of the source region by electromagnetic plasma waves traveling away from Earth, through the AKR source region. A wave traveling up the magnetic field line with a group velocity of about 1000 km s^{-1} would pass through the AKR source region (40 kHz $< f <$ 65 kHz) in about 3.5 s, in agreement with the typical observations presented in that study.

[7] *Menietti et al.* [2000] conducted a statistical survey of a semirandom sample of the AKR data observed by the plasma wave instrument (PWI) wideband receiver on board the Polar spacecraft. They determined that AKR fine-structure patterns with very narrowband, negative-drifting striations occur in approximately 6% of the high-resolution wideband spectrograms when AKR is present. Positive-sloping striations are also observed but at a much lower occurrence rate. The striations are predominantly found in the 40 kHz to 215 kHz frequency range and have a frequency extent of about 4 kHz and a typical duration less than 2 s. The majority of the striations have drift rates between -8 kHz s^{-1} and -2 kHz s^{-1} with a peak in the distribution between -6 kHz s^{-1} and -4 kHz s^{-1}. There is also a much smaller group of striations with positive drift rates of up to about 5 or 6 kHz s^{-1}.

[8] *Menietti et al.* [2000] further investigated the change of drift rate with frequency. Almost all striations are observed in the lowest two frequency bands of the wideband receiver ($f <$ 215 kHz). They found a small decrease in the statistical drift rate with increasing frequency. The frequency slope of the striations is nearly constant $df/dt \approx -5$ kHz s^{-1}.

[9] *Mutel et al.* [2006] have recently surveyed the properties of AKR ordered fine structure using the wideband data (WBD) instrument on the multisatellite Cluster spacecraft [*Gurnett et al.*, 2001]. These authors find that the signature of OFS is detected at all three observing bands (125 kHz, 250 kHz, and 500 kHz), but is observed most frequently at the lowest band (125 kHz). The frequency drifts also vary within the limits seen previously by *Menietti et al.* [2000], but some frequency drifts appear to be nonlinear. The bandwidth of individual bursts can be extremely small, perhaps 20 Hz.

2. Electromagnetic Ion-Cyclotron (EMIC) Waves

[10] EMIC waves in the auroral region are of great interest because of their ability to heat ions [cf. *Andre et al.*, 1986] and to modulate electrons [*Bergmann*, 1984; *Temerin and Lysak*, 1984; *Temerin et al.*, 1986]. These waves are known to play a major role in the generation of ion conical distributions. Inertial Alfven waves have been proposed to initiate the time-of-flight resonance with electrons forming conical electron distributions. *Wygant et al.* [2000] have presented evidence that kinetic Alfven waves that accelerate electrons are observed in the plasma sheet boundary layer at altitudes of 4 to 6 R_E. These waves may result from larger-scale Alfven waves that carry enough Poynting flux to explain intense auroral structures observed by the Polar Ultraviolet Imager data. In the past the parallel electric fields associated with intense kinetic Alfven waves (KAW) have been associated with both parallel acceleration of electrons and perpendicular heating of ions [cf. *Goertz*, 1984; *Lysak and Lotko*, 1996; *Hui and Seyler*, 1992; *Kletzing*, 1994]. Observations have been made on a number of satellites including S3-3 [*Mozer et al.*, 1980], Viking [*Block and Falthammar*, 1990], DE 1 [*Weimer and Gurnett*, 1993; *Menietti et al.*, 1994; *Menietti et al.*, 1998].

[11] *Temerin et al.* [1986], *McFadden et al.* [1998], *Lund et al.* [1998], and *Chaston et al.* [1998] have all shown the importance of EMIC waves in the acceleration and modulation of auroral particles. *Lund and LaBelle* [1997] and *Chaston et al.* [2002] have modeled wave growth of EMIC waves in and near the auroral region. These authors have relied on observations of waves with frequencies in the vicinity of the proton cyclotron frequency and its harmonics. Both electrostatic (EIC) and electromagnetic (EMIC) ion cyclotron waves are observed by FAST in the auroral acceleration region associated with upward ion beams [*Cattell et al.*, 1998; *McFadden et al.*, 1998; *Chaston et al.*, 1998]. These waves are observed with Poynting flux directed both downward and upward. The latter authors have shown that the source of these waves is the electron and ion beams observed within the auroral acceleration region. Within this region the waves are observed to have amplitudes of up to 1 V/m (E) and 2 nT (B) with E_1/B_1 ratios as small as c. *Chaston et al.* [2002] have shown that the EMIC waves grow through inverse Landau resonance with a cold field-aligned electron beam superimposed on an accelerated and magnetically mirrored plasma sheet electron component in the absence of any significant plasma densities at energies below $\sim$100 eV. These waves are modeled with parallel wavelengths $\sim$100 km or less (cf. Figure 11 of *Chaston et al.* [2002]). The upward propagating waves were the result of backward propagation and thus are still consistent with an inverse Landau growth mechanism. *Santolik et al.* [2002] found that the ratio of the amplitudes of the electric and magnetic fluctuations was usually larger than the speed of light and that the vector of the wave magnetic field was close to the plane perpendicular to the static magnetic field, corresponding to the superposition of many linearly polarized waves.

[12] In this paper we investigate the role of EMIC waves in the possible stimulation of auroral kilometric radiation. While the Polar spacecraft made numerous passes near and within the AKR source region at perigee in the Southern Hemisphere, almost none of these passes contain wideband plasma wave data in the necessary range of frequencies to observe AKR. Therefore in an effort to obtain in situ plasma particle data during times of observed AKR ordered fine structure, we searched for magnetic conjunctions between Polar and Cluster satellites when Polar was encountering the AKR source region. One such pass was found on

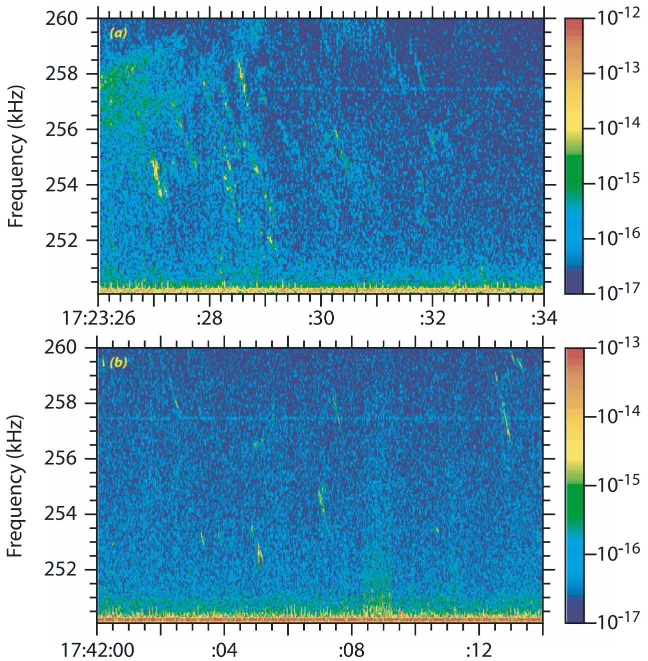

Figure 1. (a) Frequency-time spectrum observed in the 250–260 kHz band by the Cluster WBD instrument over an eight second interval starting at 1723:26 UT on 22 October 2002. Note the narrow-band striated AKR bursts which are the subject of this study. (b) Another example of striated AKR bursts starting at 1742:00 UT. During these time intervals, the electron distribution function was measured near magnetic conjunction by the HYDRA instrument on Polar (Figure 2).

22 October 2002. We model the distribution function observed by the electron and ion hot plasma instrument (HYDRA) within this AKR generation region. We show that the observed electron distribution can provide the free energy source for generation EMIC waves, which in turn, may stimulate the growth of the AKR to produce ordered fine structure as observed.

3. Observations

[13] In Figure 1a we display a frequency-time spectrogram of the high-resolution wideband wave data obtained by the WBD instrument on board the Cluster spacecraft. The data are relative intensities of the electric field data taken over an 8 s time interval starting at 1723:26 on 22 October 2002. Seen in the plot are the ordered fine structure striations which are the subject of this study. Another example seen at a later time is shown in Figure 1b. The Cluster wideband instrument was in a mode to measure frequencies from about 250 kHz to 260 kHz at the time. These data (Figure 1) were obtained high over the southern auroral region when Cluster was near 15.8 R_E, magnetic latitude of $-48°$, MLT of 20.5 hours, and L = 35.3. At about this time, 1706 (and again at 1709), the Polar spacecraft was near magnetic conjunction with Cluster. The conjunctions were determined using the software provided by the Satellite Situation Center at NASA Goddard Space Flight Center. This software uses the IGRF and Tsyganenko 1989 magnetic field models. The conjunction occurred within 2 degrees latitude and 5 degrees longitude in geographic coordinates. The Polar spacecraft particle data was obtained about 20 min earlier than the Cluster wave data observations. At 1706:00 the Polar satellite was near perigee at 3.39 R_E, 1748 hours LT, $-74.01°$ magnetic latitude, 81.4° invariant latitude, and a dipole L-value of 45.1. The satellite was believed to be near the upper edge of the auroral kilometric generation region. While the conjugacy is not perfect, we point out that the occurrence of ordered fine structure in AKR is relatively rare ($\sim$6%), and the orbit of Polar, with perigee near 2 R_E, did not provide numerous opportunities to encounter the AKR source region. Therefore the case of near-conjugacy here studied is quite fortuitous.

[14] In Figure 2 we display a contour plot of the electron distribution function in velocity space as measured by the HYDRA instrument on board the Polar spacecraft. The data for the plot were collected over approximately 12.5 s (two spins) near a magnetic conjunction between Polar and the Cluster satellite suite. The contour plot displays features of a horseshoe distribution as described by *Delory et al.* [1998] or *Menietti et al.* [1993]. These distributions are believed to be unstable to the growth of AKR under certain conditions as explained by *Pritchett et al.* [1999, 2002], for instance. Seen in Figure 2 are the downward beam-like electrons forming the curve of the horseshoe and the deep upward loss cone. The electron cyclotron frequency during this period is $f_{ce} \sim 50$ kHz, as measured using the magnetometer data, and the plasma frequency, f_p = 2520 Hz as determined from integration of the particle data from the hot plasma instrument (HYDRA). The HYDRA instrument has a low energy cutoff at about 10 eV and the spacecraft potential at the time varies from about +20 to +30 volts. Thus there

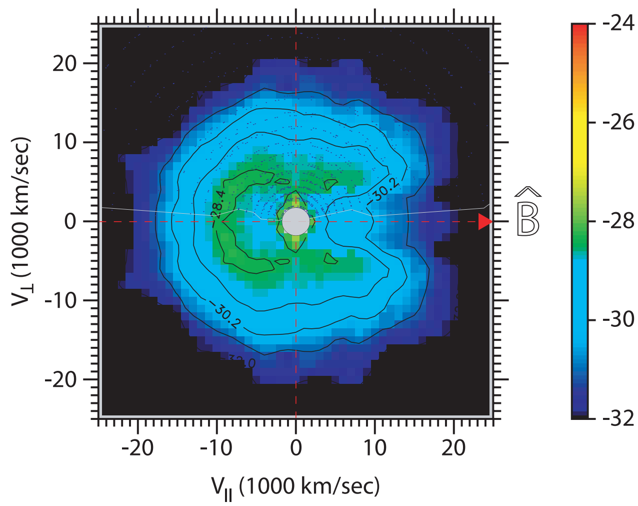

Figure 2. Contours of the phase space electron distribution obtained by HYDRA on board the Polar spacecraft. This distribution is distinguished by its characteristic "horseshoe" shape and can be unstable to AKR. This distribution is characterized by a field-aligned beam and a "shell" distribution of adiabatically distributed electrons forming the legs of the horseshoe. The data for the plot were collected over approximately 12.5 s near a magnetic conjunction between Polar and the Cluster satellite suite.

could be a missing cold plasma population, which would have some effect on the model distribution and hence the growth of the EMIC waves. We do note, however, that *Strangeway et al.* [1998] have reported that the auroral AKR source region apparently contains negligible cold plasma.

4. Model of the Electron Distribution

[15] We have attempted to model the electron phase space distribution using a sum of Maxwellian distributions as we describe below. In order to investigate the role of an electron beam in the generation of the EMIC waves, we have used a modification of a well-tested computer code, WHAMP (Waves in Homogeneous, Anisotropic Multicomponent Plasmas) [*Ronnmark*, 1982]. The modifications to the code are for diagnostics and to facilitate integration but do not affect the steps in finding the solution to the dispersion equation. WHAMP is a computer program which solves the dispersion relation of waves in a magnetized plasma. The dielectric tensor is derived using the kinetic theory of homogeneous plasmas with Maxwellian velocity distributions. Up to six different plasma components can be included (we use up to three in this work), and each component is specified by its density, temperature, particle mass, anisotropy, loss-cone depth and width, and drift velocity along the magnetic field. In this study a modified form of the distribution function introduced by *Ronnmark* [1982, 1983] is used as follows:

$$f_s(v_\perp, v_\parallel) = \sum_s \left(\frac{n_s}{\pi^{\frac{3}{2}} w_{\perp_s}^2 w_{\parallel_s}} \right) \cdot e^{-\frac{\left(v_\parallel - v_{ds}\right)^2}{w_{\parallel s}^2}} \left[(1-\Delta_s) e^{-\frac{v_\perp^2}{w_{\perp s}^2}} + \frac{\Delta_s}{(1-\beta_s)} \cdot \left(e^{-\frac{v_\perp^2}{w_{\perp s}^2}} - e^{-\frac{v_\perp^2}{\beta_s w_{\perp s}^2}} \right) \right] \quad (1)$$

where $w_\parallel$ and $w_\perp$ are the particle velocities parallel and perpendicular to the magnetic field, respectively; $v_\parallel$ and $v_\perp$ are the parallel and perpendicular thermal velocities, respectively; v_d is the parallel drift velocity. The parameters Δ and β describe the depth and width of the model loss cone, respectively.

[16] In Figure 3 we show a cartoon of a possible scenario for stimulating the growth of AKR and the ordered fine structure. Field-aligned electrons that have served to satisfy the resonance condition for the growth of AKR also serve as a free-energy source for the growth of EMIC waves near the lower part of the auroral acceleration region. These waves are generated by inverse Landau resonance as described by *Chaston et al.* [2002]. Thus most of the Poynting flux is directed downward in the same direction as the electron beam, but some emission can be directed upward as well. This emission is backward propagating with the group velocity in the opposite direction from the phase velocity. Since Landau resonance requires the close agreement of the electron velocity and the wave phase velocity, the waves still grow despite the backward group velocity propagation.

[17] As discussed by *Temerin and Lysak* [1984], the emission propagating downward will reflect near the ion hybrid frequency in a multicomponent plasma. *Rauch and Roux* [1982] and *Lund and LaBelle* [1997] have performed ray tracings of such waves. Upon reflection, this emission can penetrate the AKR source region before it is damped near the local ion cyclotron frequency (f_{cp}). However, emission for which the wave growth occurs for frequencies less than f_{cp} can propagate to altitudes higher than the wave generation region. This emission as well as the backward propagating emission may act to stimulate the growth of AKR to produce the ordered fine structure which almost always appears with negative slope (which can be explained naturally by a stimulating wave propagating away from the Earth). The EMIC waves have a group velocity that is typically several hundred km s^{-1} until the waves are near f_{cp}, at which time the group velocity decreases rapidly and the interaction of the waves and the electrons ceases. The process of AKR stimulation we believe is a result of the EMIC waves modifying the plasma distribution function or altering the ratio of f_p/f_{ce} locally to small values, thus increasing the growth rate of AKR according the cyclotron maser theory. In the next section we examine the role of the observed electron beams in the generation of the EMIC

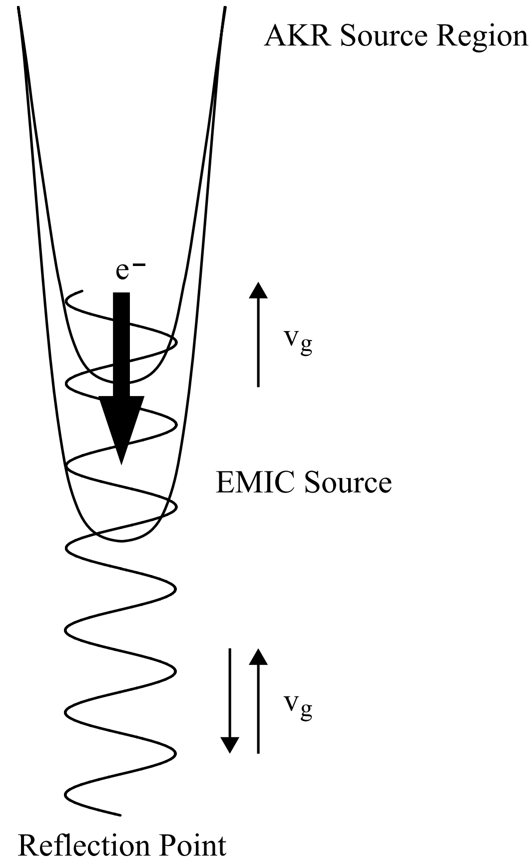

Figure 3. A cartoon scenario for stimulating the growth of AKR and the ordered fine structure. Field-aligned electrons that have served to satisfy the resonance condition for the growth of AKR also serve as a free-energy source for the growth of EMIC waves near the lower part of the auroral acceleration region. These waves can be generated in both the forward and backward directions relative to the electron beam. Downward propagating waves reflect at the ion hybrid frequency to propagate back up the magnetic field line.

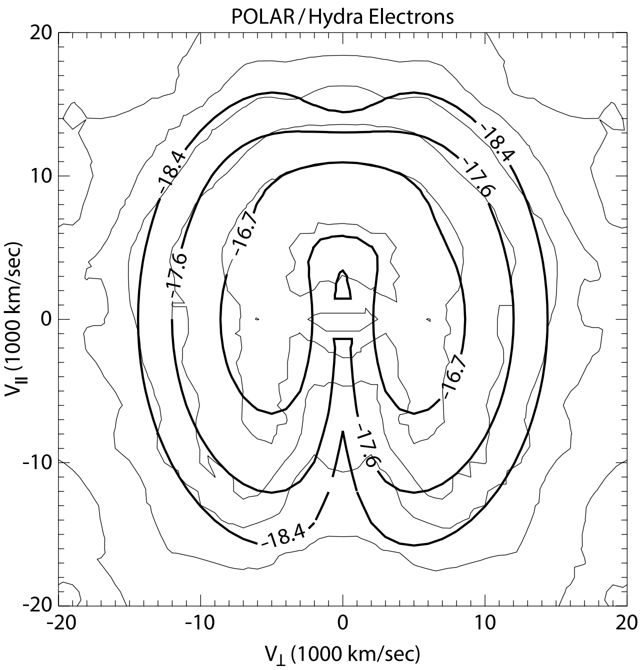

Figure 4. A model fit consisting of a background and a drifting Maxwellian with fitting parameters shown in Table 1. The fit contours overplot the HYDRA data contours seen also in Figure 2.

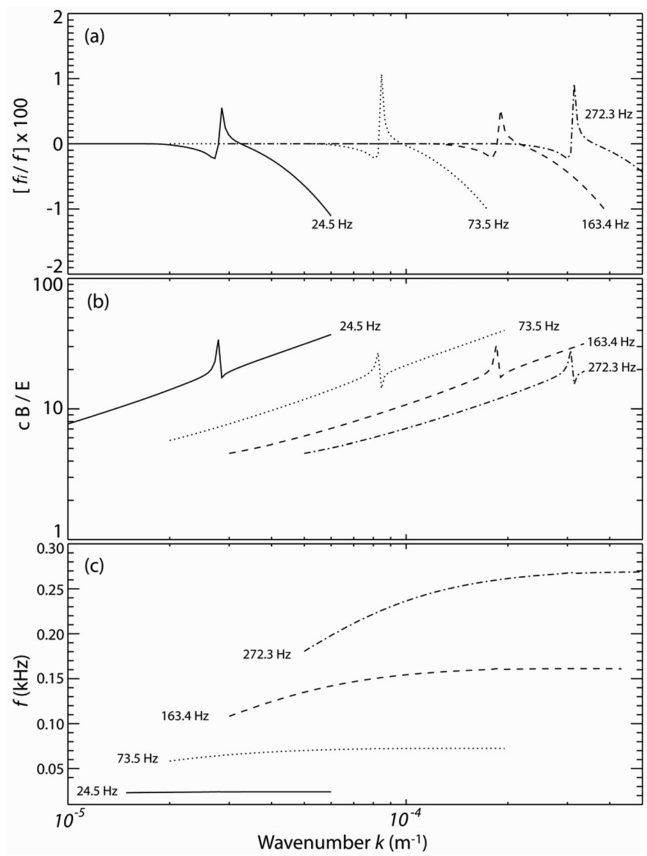

Figure 5. Multi-panel plots of the results of dispersion analysis for f_{cp} = 24.5 Hz, 73.5 Hz, 163.4 Hz, and 272.3 Hz. The wave normal angle, $\Psi = 70°$, for each example. The lower panel is the real frequency, the middle panel is cB/E and the top panel is the ratio of the imaginary frequency to real frequency expressed in percent. The abscissa for all the panels is the wave number (m^{-1}).

waves. The detailed process of wave stimulation of AKR by the EMIC waves is a subject of an ongoing investigation to be discussed in the future.

5. Generation of EMIC Waves By the Observed Electron Distribution

[18] To begin our investigation, we fit the distribution function of Figure 2 using a nonlinear least-squares fitting routine. In Figure 4 we show the model fit consisting of a background and a drifting Maxwellian with fitting parameters shown in Table 1. The parameters shown in Table 1 are those obtained from the best fit, except that we have increased the beam drift velocity from 8.0×10^6 m s^{-1} to 1.6×10^7 m s^{-1} in order to excite the growth of EMIC waves. We note again that Polar was located relatively high in the AKR source region with a substantial field-aligned potential beneath the satellite. HYDRA observed upward directed field-aligned ion beams with energies approaching 4 keV near this time period, indicating that field-aligned potentials of this magnitude were beneath the satellite at times. This would justify increasing the beam velocity by at least a factor of two for growth at lower altitudes and $f > 50$ kHz (the local cyclotron frequency during the Polar observations).

Table 1. Model Parameters for Observed Electron Distribution

Parameter	Electron Beam	Electron Shell	Ion Background
Parallel temperature, eV	49.5	285	95
Thermal velocity ratio, $w_\perp/w_\parallel$	1.67	0.767	1.00
Beam drift velocity, v_d, km s^{-1}	$1.62 \cdot 10^4$	-	-
Beam density ratio, n_b/n_0	0.036	-	-
Loss cone depth parameter, Δ	-	0.01	-
Loss cone width parameter, β	-	0.728	-
Shell density ratio, n_{sh}/n_0	-	0.964	-

[19] The parameters of Table 1 were used in the analysis of wave growth using the modified WHAMP code. We have investigated the growth of EMIC waves for a number of frequencies. In Figure 5 we display a series of plots of the results of dispersion analysis for f_{cp} = 24.5 Hz, 73.5 Hz, 163.4 Hz, and 272.3 Hz. The wave normal angle, Ψ (between the wave number vector, $\boldsymbol{k}$, and the ambient magnetic field), was held constant at 70° for each example. The lower panel is the real frequency, the middle panel is $c\,B/E$, and the top panel is the ratio of the imaginary frequency to real frequency expressed in percent. The abscissa for all the panels is the wave number (m^{-1}). Note in these plots that the growth seen in the top panel occurs near the ion cyclotron frequency. The growth is moderate and occurs near $\omega \cdot \cos\Psi \sim k\,v_b$ as expected for the inverse Landau interaction. In Figure 6 we show the effect of changing the wave normal angle from 30° to 80° while holding f_{cp} = 73.5 Hz. The effect observed is that the wave growth increases with wave normal angle and the maximum growth shifts in k so that $\omega \cdot \cos\Psi \sim k\,v_b$ is maintained. The maximum growth occurs for $f_{max} \lesssim f_{cp}$, but f_{max} decreases with increasing wave normal angle.

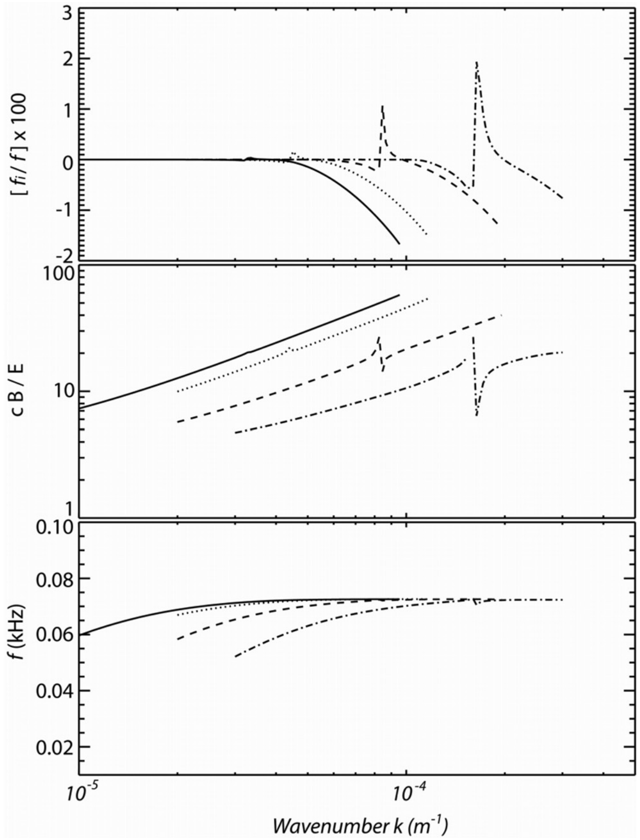

Figure 6. A plot of relative wave growth rate versus k for varying wave normal angles $\Psi = 30°$ (solid line), 50° (dotted line), 70° (dashed line), and 80° (dash-dotted line) for constant ion cyclotron frequency f_{cp} = 73.5 Hz. Wave growth increases with wave normal angle and the maximum growth shifts in k so that $\omega \sim kv_b$ is maintained.

[20] In Figure 7 we plot $100 \times (f_{cp} - f_{\max})/f_{cp}$ versus Ψ for the case of f_{cp} = 73.5 Hz. Note the curve increases with the fractional frequency difference reaching a peak at about 0.13 at $\Psi = 85°$. This indicates that we can expect wave growth over a spread of frequencies near and less than f_{cp}.

[21] For each case of f_{cp} we have calculated the group velocity as a function of frequency for $\psi = 70°$. The maximum group velocity usually occurs very near the frequency of maximum growth rate and then decreases with frequency. We have determined the median value of the group velocity for those frequencies for which wave growth occurs. Table 2 lists these values for each case of f_{cp}. As seen, the values are all in the range of 300 to 400 km/s.

[22] We have found that mildly increasing the beam velocity tends to decrease the growth rate a bit but also produces a group velocity in the opposite direction of the electron beam. That is, the wave is backward propagating relative to k and the phase velocity for a limited number of frequencies. We have increased the electron beam velocity by 6.2% to 1.72×10^7 km/s for all four cases of f_{cp}. The effect is to decrease the wave growth from 40%–70% and produce a negative wave propagation for a limited range of frequencies and wave numbers close to the frequency of maximum wave growth. We note that *Chaston et al.* [2002] performed a more extensive parameter search and found a region of negative propagation (cf. their Figure 6f). This effect is displayed in Figure 8 for the case of f_{cp} = 163.4 Hz, where we show a close-up plot of f versus k near the point of maximum growth. The slope of the dispersion curve has a negative portion, i.e., the wave is backward propagating near the point of maximum growth. The growth rate is shown in Figure 8 by the dashed curve. The other cases of f_{cp} all look similar. The values of V_g for these backward propagating waves for all four cases are also listed in Table 2.

[23] The frequency drifts measured on Figures 1a and 1b vary from about −4.5 kHz/s to as high as −13.3 kHz/s. For a dipole magnetic field this would suggest a source region (for $f_{cp} \sim 256$ kHz) at about 1.84 R_E, drifting up the magnetic field line in the range of 70 km/s to 200 km/s. The forward group velocities calculated for the EMIC waves are higher than these values by a factor of 2 to 3, while the values of V_g for the backward propagating waves are closer. This discrepancy is within the margin expected for reasonable variations of the model parameters of Table 1.

6. Summary and Conclusions

[24] We have investigated the growth of EMIC waves due to electron beams within an AKR source region based on observations during a near conjunction of the Polar spacecraft (within the AKR source region near 3.4 R_E) and the Cluster C1 satellite at approximately 15 R_E above. The near conjunction is significant because it occurs at a time when the wideband instrument on board C1 observed AKR with embedded striated fine structure. We have used the plasma particle observations of HYDRA on board Polar to determine if the growth of EMIC waves is possible at this time. We hypothesize that the EMIC waves have a significant role to play in the stimulation of AKR wave growth and the formation of the ordered fine structure.

[25] Polar was located at the upper extent of the traditional AKR source region with a local value of $f_{ce} \sim 50$ kHz. The HYDRA observations show the presence of horseshoe distributions at this altitude and it is the electron beam of this distribution that provides the free energy for the growth of EMIC waves at a lower altitude. We have multiplied the observed beam energy by a factor of 2 in order to allow the growth of EMIC waves that might be observed at lower altitudes (enhanced the energy by a factor of 4). This seems reasonable because we observe upward ion beams that extend in energy to over 4 keV at the same time that downward electrons have a maximum energy of about 1 keV.

[26] The results of this study of the wave growth for a number of frequencies indicates that EMIC waves do grow over a range of frequencies less than the local value of f_{cp}. The waves display forward and backward propagating group velocities that are in the range of several hundred km s^{-1}. Downward propagating waves reflect at the multi-ion hybrid frequency to propagate back up the field line and into the AKR wave growth region. Those waves which grow for $(f_{cp} - f)/f_{cp} \sim 0.1$ could be expected to penetrate the AKR source region for a range of frequencies extending several kHz. This would be in agreement with observations of OFS which show the signatures typically extending for several kHz. For the case of f_{cp} = 163.4 Hz, for instance, upward propagation occurs near f = 160.44 Hz or $(f_{cp} - f)$ =

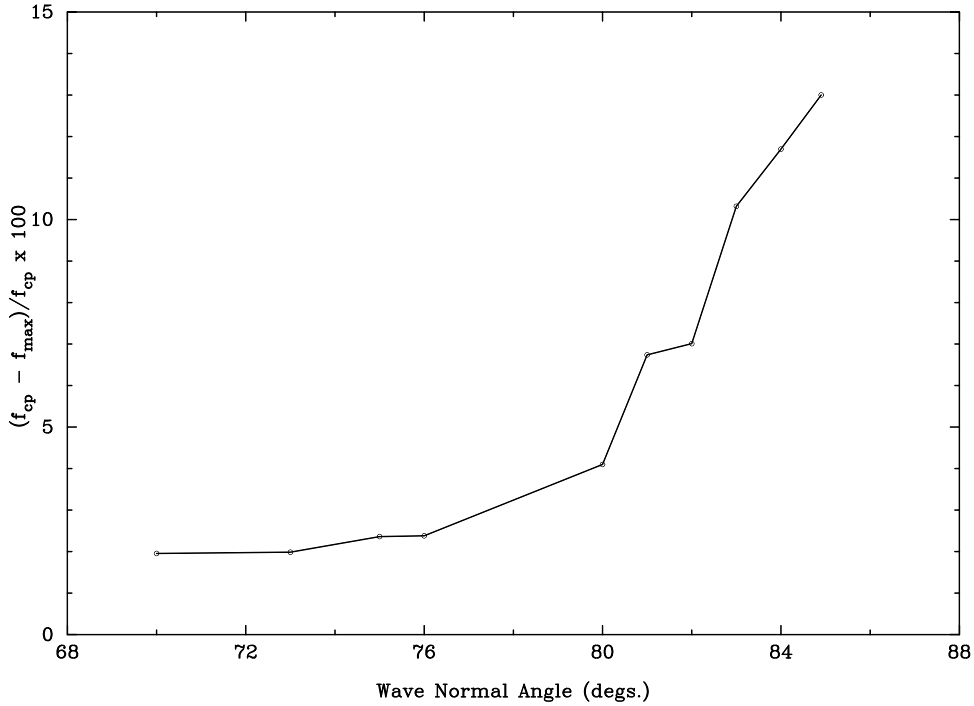

Figure 7. Fractional frequency difference $(f_{cp} - f_{\max})/f_{cp}$ vs. wave normal angle Ψ for the case of f_{cp} = 73.5 Hz. Note the curve increases with wave number reaching a peak at about 0.13 at $\Psi = 85°$. This indicates that we can expect wave growth over a spread of frequencies near and less than f_{cp}.

0.018, which would allow propagation up the field line from the point of growth near f_{cp} of perhaps 70 km. The corresponding range of electron cyclotron frequencies would be over 5 kHz. This is the observed frequency extent of many examples of striations (rain).

[27] Observations of ordered fine structure indicate a definite dominance of negative versus positive slope of frequency drifting signatures. For these cases, it is clear that only EMIC waves that propagate in the antielectron beam direction (away from Earth) influence the AKR wave growth. These presumably are those waves that are backward propagating or that have been generated by earthward electron beams and are reflected at the multi-ion-hybrid frequency. One possible reason why the downgoing waves do not often stimulate AKR wave growth is that they are generated below the AKR source region and propagate down, away from it. The energy source of the EMIC waves is the electron beam, which is best developed at the bottom of the AKR source region. The reflected waves can propagate back up into the AKR growth region if they were generated at $f < f_{cp}$. In addition, the waves traveling down the field line toward Earth interact efficiently with the downward electron beam due to inverse Landau resonance and beam energy is lost to the growth of EMIC waves. Reflected waves do not interact with the electron beam efficiently but can interact with electrons at large and negative pitch angles. They can thus possibly modify the electron distribution function or lower the ratio f_p/f_{ce} in the AKR source region and trigger the growth of AKR. Ordered fine structure seems to occur more frequently at lower frequencies (higher altitudes). EMIC waves are thought to be generated most efficiently at lower altitudes within the AKR source region. This could be problematic for the model of EMIC-generated OFS. One solution might be that occasionally (<10% of the time) EMIC waves are generated at higher altitudes when the electron beams are well developed there. Recall that OFS occurs less than 10% of the time that AKR is observed. Another interesting alternative, one that is not investigated in this study, is the generation of upward propagating EMIC waves via inverse Landau damping resulting from the upward accelerated ion beams seen near the top of the upward current region. *Bergmann* [1984] has shown that EIC waves are unstable to upward ion beams when $T_e > T_i$. The fact that each individual frequency drifting feature has a very narrow bandwidth (~20 Hz), however, is not directly explainable by the stimulation of AKR via EMIC waves but perhaps could be with much shorter wavelength EIC waves resulting from nonlinear processes. Details of the triggering mechanism thus remain to be investigated.

[28] We have considered the stimulation of AKR by EMIC waves as a possible explanation of ordered fine structure. *Pottelette et al.* [2001] have presented a theory based on electron holes to explain typical or random fine structure of AKR. The unique characteristics of ordered fine structure (rain) seem to argue against electron holes. Electron holes are much more commonly observed in the downward

Table 2. Wave Group Velocity

f_{cp}	V_g, km/s $V_d = 1.62 \times 10^4$ km/s	Backward V_g, km/s $V_d = 1.72 \times 10^4$ km/s
24.5 Hz	380	−158
73.5 Hz	377	−230
163.4 Hz	379	−165
272.3 Hz	400	−211

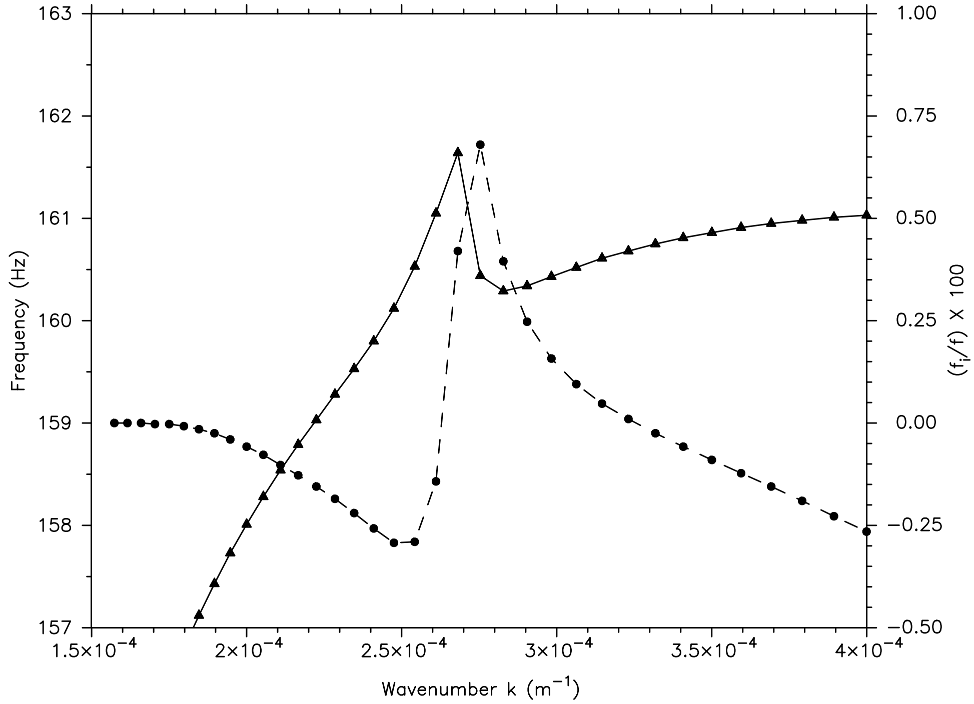

Figure 8. A close-up plot of f versus k near the point of maximum wave growth for the case of f_{cp} = 163.39 Hz. Growth proceeds for a small range of wave numbers beyond the maximum frequency (solid curve) as seen in the dashed curve (right-hand scale) which displays the growth rate. Note the slope of the dispersion curve is negative near the point of maximum wave growth yielding $V_g = -165$ km s^{-1}.

current region and have observed velocities which are larger (∼5000 km/s) than the velocities required by the observed frequency drift rates [*Ergun et al.*, 1998b; *Bounds et al.*, 1999]. Ion holes or the more recently discovered tripolar structures within the upward current region [*Pottelette and Treumann*, 2005] offer an intriguing alternative model for the production of ordered fine structure. Such structures can have velocities that depend on the difference between the ion beam velocity and the ion acoustic phase velocity. These velocities can be several hundred km s^{-1}, in agreement with the fine structure frequency drifts. In addition, ion holes and tripolar structures have widths of a few milliseconds. For estimated drift velocities this would correspond to structure sizes of only several hundred meters. This small size could be consistent with the small bandwidths of AKR ordered fine structure of ∼20 Hz [*Mutel et al.*, 2006]. To date, no correspondence between the observation of ordered fine structure and ion holes or tripolar structures has been made. In addition, the effectiveness of the possible stimulation of AKR by EMIC waves and/or ion holes/tripolar structures is a topic of ongoing research.

[29] **Acknowledgments.** This research was supported by the NASA Goddard Space Flight Center under grants NAG5-9974, NNG04GB98G, NAG5-11942, and NNG05GC28G and by the NSF awards ATM-0407155 and INT-0307319. We wish to thank J. Hospodarsky for text editing and A. Persoon for graphic assistance.

[30] Lou-Chuang Lee thanks the reviewers for their assistance in evaluating this paper.

References

Andre, M., M. Temerin, and D. Gorney (1986), Resonant generation of ion waves on auroral field lines by positive slopes in ion velocity space, *J. Geophys. Res.*, *91*, 3145–3151.

Benson, R. F., M. M. Mellott, R. L. Huff, and D. A. Gurnett (1988), Ordinary mode auroral kilometric radiation fine structure observed by DE-1, *J. Geophys. Res.*, *93*, 7515–7520.

Bergmann, R. (1984), Electrostatic ion (hydrogen) cyclotron and ion acoustic wave instabilities in regions of upward field-aligned current and upward ion beams, *J. Geophys. Res.*, *89*, 953–968.

Block, L. P., and C.-G. Falthammar (1990), The role of magnetic-field-aligned electric fields in auroral acceleration, *J. Geophys. Res.*, *95*, 5877–5888.

Bounds, S. R., R. F. Pfaff, S. F. Knowlton, F. S. Mozer, M. A. Temerin, and C. A. Kletzing (1999), Solitary potential structures associated with ion and electron beams near 1 R_E altitude, *J. Geophys. Res.*, *104*, 28,709–28,717.

Cattell, C., et al. (1998), The association of electrostatic ion cyclotron waves, ion and electron beams and field-aligned currents: FAST observations of an auroral zone crossing near midnight, *Geophys. Res. Lett.*, *25*, 2053–2056.

Chaston, C. C., et al. (1998), Characteristics of electromagnetic proton cyclotron waves along auroral field lines observed by FAST in regions of upward current, *Geophys. Res. Lett.*, *25*, 2057–2060.

Chaston, C. C., J. W. Bonnell, J. P. McFadden, R. E. Ergun, and C. W. Carlson (2002), Electromagnetic ion cyclotron waves at proton cyclotron harmonics, *J. Geophys. Res.*, *107*(A11), 1351, doi:10.1029/2001JA900141.

Delory, G. T., R. E. Ergun, C. W. Carlson, L. Muschietti, C. C. Chaston, W. Peria, J. P. McFadden, and R. Strangeway (1998), FAST observations of electron distributions within AKR source regions, *Geophys. Res. Lett.*, *25*, 2069–2072.

Ergun, R. E., et al. (1998a), FAST satellite wave observations in the AKR source region, *Geophys. Res. Lett.*, *25*, 2061–2064.

Ergun, R. E., et al. (1998b), FAST satellite observations of large-amplitude solitary structures, *Geophys. Res. Lett.*, *25*, 2041–2044.

Ergun, R. E., C. W. Carlson, L. Muschietti, I. Roth, and J. P. McFadden (1999), Properties of fast solitary structures, *Nonlinear Proc. Geophys.*, *6*, 187–194.

Goertz, C. K. (1984), Kinetic Alfven waves on auroral field lines, *Planet. Space Sci.*, *32*, 1387–1392.

Gurnett, D. A., and R. R. Anderson (1981), The kilometric radio emission spectrum: Relationship to auroral acceleration processes, in *Physics of Auroral Arc Formation, Geophys. Monogr. Ser.*, *25*, edited by S.-I. Akasofu, and J. R. Kan, pp. 341–350, AGU, Washington, D. C.

Gurnett, D. A., R. R. Anderson, F. L. Scarf, R. W. Fredericks, and E. J. Smith (1979), Initial results from the ISEE 1 and 2 plasma wave investigation, *Space Sci. Rev.*, *23*, 103–122.

Gurnett, D. A., et al. (2001), First results from the Cluster wideband plasma wave investigation, *Ann. Geophys.*, *19*, 1259–1271.
Hui, C.-H., and C. E. Seyler (1992), Electron acceleration by Alfven waves in the magnetosphere, *J. Geophys. Res.*, *97*, 3953–3963.
Kellogg, P. J., and S. J. Monson (1979), Radio emissions from the aurora, *Geophys. Res. Lett.*, *6*, 297–300.
Kletzing, C. A. (1994), Electron acceleration by kinetic Alfven waves, *J. Geophys. Res.*, *99*, 11,095–11,104.
LaBelle, J., M. L. Trimpi, R. Brittain, and A. T. Weatherwax (1995), Fine structure of auroral ROAR emissions, *J. Geophys. Res.*, *100*, 21,953–21,959.
Lund, E. J., and J. LaBelle (1997), On the generation and propagation of auroral electromagnetic ion cyclotron waves, *J. Geophys. Res.*, *102*, 17,241–17,253.
Lund, E. J., et al. (1998), FAST observations of preferentially accelerated He+ in association with auroral electromagnetic ion cyclotron waves, *Geophys. Res. Lett.*, *25*, 2049–2052.
Lysak, R. L., and W. Lotko (1996), On the kinetic dispersion relation for shear Alfven waves, *J. Geophys. Res.*, *101*, 5085–5094.
McFadden, J. P., et al. (1998), Electron modulation and ion cyclotron waves observed by FAST, *Geophys. Res. Lett.*, *25*, 2045–2048.
Melrose, D. B. (1986), A phase-bunching mechanism for fine structures in auroral kilometric radiation and Jovian decametric radiation, *J. Geophys. Res.*, *91*, 7970–7980.
Menietti, J. D., J. L. Burch, R. M. Winglee, and D. A. Gurnett (1993), DE 1 particle and wave observations in auroral kilometric radiation (AKR) source regions, *J. Geophys. Res.*, *98*, 5865–5879.
Menietti, J. D., D. R. Weimer, M. Andre, and L. Eliasson (1994), DE 1 and Viking observations associated with electron conical distributions, *J. Geophys. Res.*, *99*, 23,673–23,684.
Menietti, J. D., H. K. Wong, W. S. Kurth, D. A. Gurnett, L. J. Granroth, and J. B. Groene (1996), Discrete, stimulated auroral kilometric radiation observed in the Galileo and DE 1 wideband data, *J. Geophys. Res.*, *101*, 10,673–10,680.
Menietti, J. D., T. F. Averkamp, D. L. Kirchner, J. S. Pickett, A. M. Persoon, and D. A. Gurnett (1998), Polar plasma wave observations in the auroral region and polar cap, in *Physics of Space Plasmas*, edited by T. Chang and J. R. Jasperse, pp. 249–254, MIT Cent. for Theor. Geo/Cosmo Plasma Phys., Cambridge, Mass.
Menietti, J. D., A. M. Persoon, J. S. Pickett, and D. A. Gurnett (2000), Statistical study of auroral kilometric radiation fine structure striations observed by Polar, *J. Geophys. Res.*, *105*, 18,857–18,866.
Morioka, A., H. Oya, and S. Miyatake (1981), Terrestrial kilometric radiation observed by satellite JIKKIKEN (EXOS-B), *J. Geomagn. Geoelectr.*, *33*, 37–62.
Mozer, F. S., C. A. Cattell, M. K. Hudson, R. L. Lysak, M. Temerin, and R. B. Torbert (1980), Satellite measurements and theories of low altitude auroral particle acceleration, *Space Sci. Rev.*, *27*, 155–213.
Mutel, R. L., J. D. Menietti, I. Christopher, D. A. Gurnett, J. Cook, and H. Frey (2006), Recent Cluster wideband studies of auroral kilometric radiation, in *Proceedings of the Cluster and Double Star Symposium*—5th *Anniversary of Cluster in Space*, edited by K. Fletcher, *Eur. Space Agency Spec. Publ., ESA SP-598*.
Pottelette, R., and R. A. Treumann (2005), Electron holes in the auroral upward current region, *Geophys. Res. Lett.*, *32*, L12104, doi:10.1029/2005GL022547.
Pottelette, R., R. E. Ergun, R. A. Treumann, M. Berthomier, C. W. Carlson, J. P. McFadden, and I. Roth (1999), Modulated electron acoustic in auroral density cavities: FAST observations, *Geophys. Res. Lett.*, *26*, 2629–2632.
Pottelette, R., R. A. Treumann, and M. Berthomier (2001), Auroral plasma turbulence and the cause of auroral kilometric radiation fine structure, *J. Geophys. Res.*, *106*, 8465–8476.
Pritchett, P. L., R. J. Strangeway, C. W. Carlson, R. E. Ergun, J. P. McFadden, and G. T. Delory (1999), Free energy sources and frequency bandwidth for the auroral kilometric radiation, *J. Geophys. Res.*, *104*, 10,317–10,326.
Pritchett, P. L., R. J. Strangeway, R. E. Ergun, and C. W. Carlson (2002), Generation and propagation of cyclotron maser emissions in the finite auroral kilometric radiation source cavity, *J. Geophys. Res.*, *107*(A12), 1437, doi:10.1029/2002JA009403.
Rauch, J. L., and A. Roux (1982), Ray tracing of VLF waves in a multicomponent magnetospheric plasma: Consequences for the generation mechanism of ion cyclotron waves, *J. Geophys. Res.*, *87*, 8191–8198.
Ronnmark, K. (1982), WHAMP-waves in a homogeneous, anisotropic, multicomponent plasma, *Rep. 179*, Kiruna Geophys. Inst., Kiruna, Sweden.
Ronnmark, K. (1983), Computation of the dielectric tensor of a Maxwellian plasma, *Plasma Phys.*, *25*, 699–701.
Santolik, O., J. S. Pickett, D. A. Gurnett, and L. R. O. Storey (2002), Magnetic component of narrow-band ion cyclotron waves in the auroral zone, *J. Geophys. Res.*, *107*(A12), 1444, doi:10.1029/2001JA000146.
Shepherd, S., J. LaBelle, M. Trimpi, and R. Brittain (1996), Auroral ROAR fine structure, in *Planetary Radio Emissions IV*, edited by H. O. Rucker, S. J. Bauer, and M. L. Kaiser, pp. 291–292, Aust. Acad. of Sci., Vienna, Austria.
Strangeway, R. J., et al. (1998), FAST observations of VLF waves in the auroral zone: Evidence of very low plasma densities, *Geophys. Res. Lett.*, *25*, 2065–2068.
Temerin, M., and R. L. Lysak (1984), Electromagnetic ion cyclotron (ELF) waves generated by auroral electron precipitation, *J. Geophys. Res.*, *89*, 2849–2859.
Temerin, M., J. P. McFadden, M. Boehm, C. W. Carlson, and W. Lotko (1986), Production of flickering aurora and field-aligned electron flux by electromagnetic ion cyclotron waves, *J. Geophys. Res.*, *91*, 5769–5792.
Wu, C. S., and L. C. Lee (1979), A theory of the terrestrial kilometric radiation, *Astrophys. J.*, *230*, 621–626.
Wygant, J. R., et al. (2000), Polar spacecraft based comparisons of intense electric fields and Poynting flux near and within the plasma sheet-tail lobe boundary to UVI images: An energy source for the aurora, *J. Geophys. Res.*, *105*, 18,675–18,692.
Weimer, D. R., and D. A. Gurnett (1993), Large amplitude auroral electric fields measured with DE-1, *J. Geophys. Res.*, *98*, 13,557–13,564.

I. W. Christopher, J. M. Cook, J. D. Menietti, R. L. Mutel, and J. D. Scudder, Department of Physics and Astronomy, University of Iowa, 203 Van Allen Hall, Iowa City, IA 52242-1479, USA. (jdm@space.physics.uiowa.edu)

O. Santolik, Faculty of Mathematics and Physics, Charles University, KEVF MFF, V Holesovickach 2, Prague 8, CZ-18000, Czech Republic.